Journal of Materials Sciences and Applications
2017; 3(6): 94-101
http://www.aascit.org/journal/jmsa
ISSN: 2381-0998 (Print); ISSN: 2381-1005 (Online)

American Association for Science and Technology

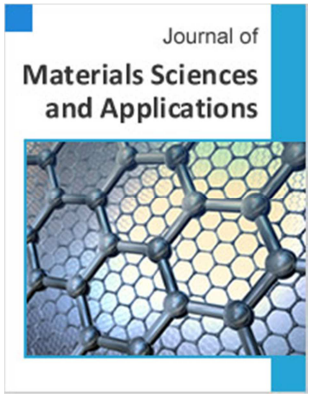

Keywords
Memristive Structure,
Thermal Oxidation,
Prof. Chua's Theory

Received: September 18, 2017
Accepted: November 14, 2017
Published: December 5, 2017

Memristive Structures Based on Thermally Oxidized TiO_x

Alejandro Avila Garcia*, Luis Ortega Reyes, Gabriel Romero-Paredes, Yuriy Koudriatsev

Department of Electrical Engineering, Center of Research and Advanced Studies, Mexico City, Mexico

Email address

aavila@cinvestav.mx (A. A. Garcia)

*Corresponding author

Citation

Alejandro Avila Garcia, Luis Ortega Reyes, Gabriel Romero-Paredes, Yuriy Koudriatsev. Memristive Structures Based on Thermally Oxidized TiO_x. *Journal of Materials Sciences and Applications.* Vol. 3, No. 6, 2017, pp. 94-101.

Abstract

Metal-insulator-metal (MIM) structures based on non-homogeneous titanium oxide films obtained by thermal oxidation of titanium metallic films were built. Oxygen and titanium concentrations are variable within the films, but a rutile structure is resembled. Digitized current-voltage measurements at room temperature under sinusoidal voltage showed hysteretic behavior. Although none memristive specific model was fitted to the electric data, the basic expressions established by Prof. Chua for the foreseen memristor yielded a detailed description of charge, magnetic flux and memristance along with their evolution during some of the first measurements. The constitutive Flux-Charge and Memristance State-map relationships of our typical device were also derived. The inverse of the experimental constitutive relationship was fitted to a double sigmoidal function. This dependence allowed describing the behavior of the same structure under different biasing waveforms: square, triangular and sawtooth. The largest memristance span turned out from the square waveform. Exponential time-dependences of the resistance between about 5 and 164 kΩ under ± 2 voltages were determined. The process used, which was based on simple spreadsheet calculations can be applied to any experimental memristive device to observe its basic performance and lead to further analysis in terms of some specific model.

1. Introduction

Plenty of resistive switching phenomena on different materials was reported during a long period [1, 2, 3, 4, 5, 6] before Strukov et al [7] ascribed to a previously predicted device called memristor [8], this type of behavior. They also proposed an electronic-ionic conduction model for explaining such properties in the case of titanium oxide-based devices [7]. Since then, many works on fabrication, modeling and applications have appeared [9, 10, 11]. Nevertheless, no one so far has departed from the theoretical view proposed by Prof. Chua as the analysis tool to describe experimental devices.

Titanium oxide films for memristive devices have been produced by several methods. Most of them were deposited by sputtering [12, 13]. Some other use more sophisticated methods like atomic layer deposition or pulsed laser deposition [14, 15]. A few of them have explored a simple and direct process including the vacuum evaporation of a titanium thin layer upon an appropriate substrate and further oxidation under a thermal treatment in air [16, 17].

Recently, the authors have studied memristive structures based on thermally oxidized

titanium and vanadium layers [18, 19].

In this work, similar memristive structures based on non-homogeneous titanium oxide were built after providing some basic characterization of the active oxide layer. Besides fabricating the structures, the aim of this work is just studying their electrical behavior for the assessment of the fabrication conditions and later achievement of reproducibility. Experimental current values under a digitized sinewave biasing voltage were acquired. Although diverse models have been proposed for explaining memristive behavior [7, 20, 21, 22], we describe the important variables ascribed to memristive behavior according to the basic definition from Prof. Chua, who first foresaw the existence of the memristor and theoretically established its main properties [8].

We illustrate how Prof. Chua's proposal can be used to extract the associated variables involved in such analysis. By following that theory, using the I-V data and the time dependence of the biasing signal, we numerically calculated the variables related to the structure behavior, as functions of time: charge, magnetic flux and memristance. Then, both the so-called constitutive relationship (magnetic flux vs. charge) and state map (memristance vs. charge) of such structures at different stages of its evolution were determined. This analysis was carried out for several I-V data sets resulting from different measurements under the same biasing signal. On the basis of these results, a description of the structure behavior during some of the first 100 cycles of biasing is presented. After the 50th measurement the I-V plots exhibited some stability, hence a functional dependence was fitted to the inverse constitutive relationship of the 100th cycle. Next, by using this functional dependence, the behavior of such structure under different voltage waveforms could be described. The behavior of the same sample under these distinct waveforms is also deduced on this basis.

2. Sample Structure and Active Layer

The structure of the samples is as used in former works of the authors. A schematic view is presented in Figure 1.

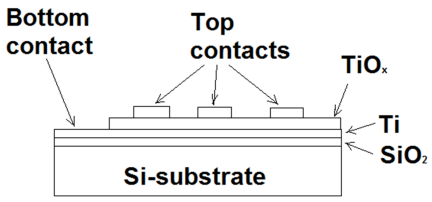

Figure 1. *Schematic structure of the samples studied in this work. The top contacts are gold evaporated dots around 1 mm diameter. The bottom contact consists of the non-oxidized titanium layer remaining below the titanium oxide film.*

The procedure for fabricating this structure is as follows: a thin titanium layer was vacuum evaporated upon the oxidized silicon substrate; then, the sample was put upon a heated plate in atmospheric air during a certain time to produce oxidation of the film; under the conditions used, some part of the metallic film was not oxidized. The result is an oxide layer containing a non-homogeneous oxygen concentration along the depth, placed upon a metallic titanium layer. Indeed, from the diffusive processes occurring during oxidation, a large concentration of oxygen near the top surface and a lower one close to the metal-oxide interface are expected. Hence, a larger concentration of oxygen vacancies near the bottom interface is also expected. These assertions can be confirmed in Figure 2, where the titanium and oxygen concentration profiles obtained from Secondary Ion Mass Spectroscopy (SIMS) measurements are showed [24]. An ims-6f Cameca France system was used to get this information. Also, at the right-hand side scale, the oxygen-titanium ratio is depicted, as compared to the accurate ratio of the rutile phase (horizontal full line).

Thickness was determined by ellipsometry measurements, carried out with a Gäertner L2W16S366 variable angle ellipsometer. In this work, a structure made with a 35 nm thick oxide was used.

Detailed observation of the [O]/[Ti] curve allows seeing that between 30 and 35 nm from the surface such ratio is about 1.97. Hence, a layer about 5 nm out of the total 35 nm oxide in the bottom of our structure in Figure 1 has a vacancy concentration adequate to produce ion drift effects [7].

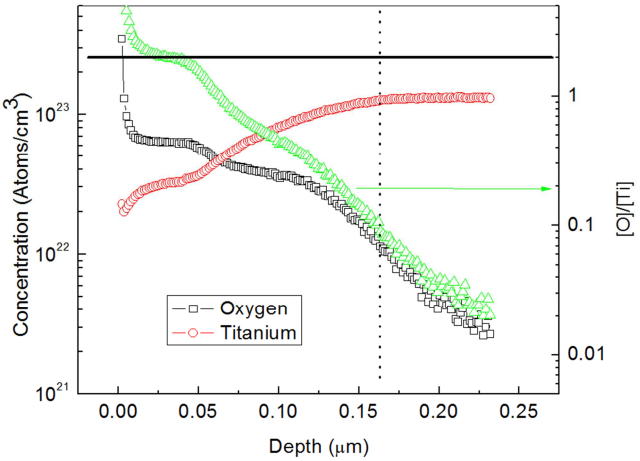

Figure 2. *SIMS spectra showing how the Ti and O concentrations vary along the depth of an oxidized Ti film. This is the result corresponding to a film about 150 nm thick, oxidized at 550°C during 40 minutes. The vertical dashed line indicates the approximate thickness value of the oxide film.*

Some information on the chemical composition is given by the Raman spectrum in Figure 3, which was obtained at room temperature with an HR800 model Horiba-Jobin Yvon equipment. The 460.5 and 623.5 cm^{-1} bands are identified as shifted from the characteristic rutile bands found at 448 cm^{-1} (E_g) and 612 cm^{-1} (A_{1g}) respectively [25]. The 247.5 band is ascribed to either scattering between two phonons or high disorder [26]. The 161.7 cm^{-1} band might correspond to either rutile or anatase phases or a combination of them [27]. Despite the disorder introduced by the non-homogeneity of oxygen and titanium, the oxide grows under a specific trend: it tends towards the rutile structure which is not unexpected. Nevertheless, the important fact for achieving the memristive

effect becomes the non-homogeneity of oxygen vacancies, according to Strukov et al [7]. Moreover, a film with a large concentration of defects would favor diffusion of ionic defects, whatever these may be: either oxygen vacancies or any other type. This in turn would favor the observation of the expected hysteresis effect in the current-voltage curves of these structures.

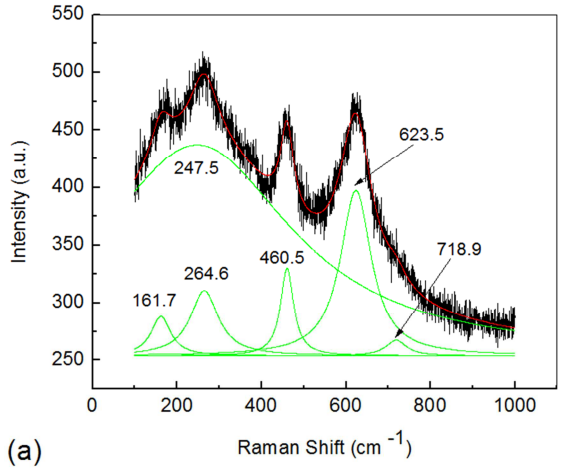

Figure 3. *Raman spectrum of an oxide layer oxidized at 550°C during 30 minutes, showing the bands that were numerically deconvoluted.*

3. Electrical Measurements

Current-Voltage measurements were carried out at room temperature by using a Keithley 4200 Semiconductor Characterization System.

The biasing signal was a digitized sinusoidal wave given as:

$$V(t) = A\sin(\omega t + \pi) \qquad (1)$$

Where A is the voltage amplitude (2 V) and ω the angular frequency given as ω = 2π/T, being T the cycle period (T = 34 s).

More than one hundred cycles of this waveform were applied to the sample and the corresponding current values recorded. A positive voltage means that the higher potential is applied to the bottom contact of our structure. The voltage in equation (1) implies that the negative semi-cycle was first applied in all the measurements whose results are discussed. For the sake of clearness, we only show the results of the 1st, 2nd, 3rd, 6th, 9th, 50th and 100th cycles as typical values during different stages of the sample evolution.

The I-V plots corresponding to the cycles above mentioned are shown in Figure 4. Each cycle was digitized by acquiring 4096 current-voltage pairs. The I-V curves are grouped in three parts according to their similarities regarding shape and current values. The 1st, 2nd and 3rd cycles are characterized by instability, nevertheless hysteresis can be seen. They are shown together in the top part of Figure 4. In the 6th and 9th cycles this instability decreases, but still the magnitude of current mainly in the positive semi-cycle undergoes a significant evolution. This is shown in the middle part of Figure 4. Finally, the 50th and 100th cycles exhibit more stability, but hysteresis is less noticeable. These last curves are the result of a sort of final state of the structure with rather reproducible response to the same exciting voltage signal. Also, some degree of asymmetry between positive and negative voltages can be seen from the first up to the final plots. The structure was led from a highly resistive state at the beginning, towards a less resistive state at the last cycles. At this point it is worthwhile stressing that, according to Prof. Chua, hysteresis is the distinctive characteristic for a memristive device [23].

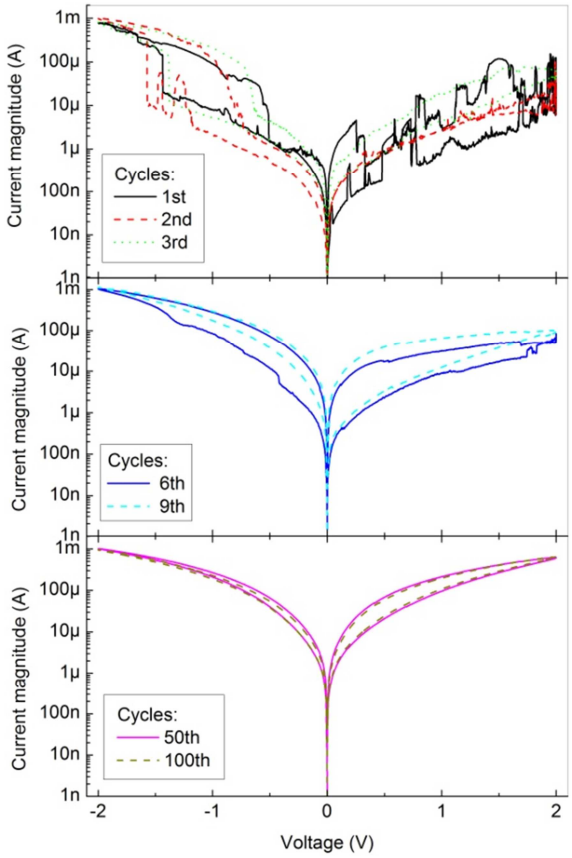

Figure 4. *Semi-logarithmic I-V plots exhibiting hysteresis, obtained under a sinewave excitation voltage starting from zero towards negative voltages. Top: The first 3 cycles. Middle: 6th and 9th cycles. Bottom: 50th and 100th cycles.*

In Figure 4 the maximum magnitude of the current for negative voltages remains the same (~ 1 mA) for all these results, but hysteresis undergoes some change. For positive voltage both, the hysteresis and the maximum current evolve along the measurements. Currents for voltages close to zero significantly increase as the measurements run, indicating smaller resistances. This fact decreases the resistance (memristance) span, as it will be shown later. Although a clear evolution of the structure exists, this is seen to include soft changes, i.e. none hard forming process is needed upon these structures.

In Figure 5 the important variables are plotted as functions of time. Apart from the voltage, all of them were numerically calculated. At the top part both the original voltage sine

waveform used during each cycle (black line) and the associated magnetic flux (red line), which was calculated by the time integration of the voltage as proposed by Chua [8]:

$$\varphi(t) = \int_0^t V(x)\,dx \qquad (2)$$

are depicted. These two signals are the same for all the cycles.

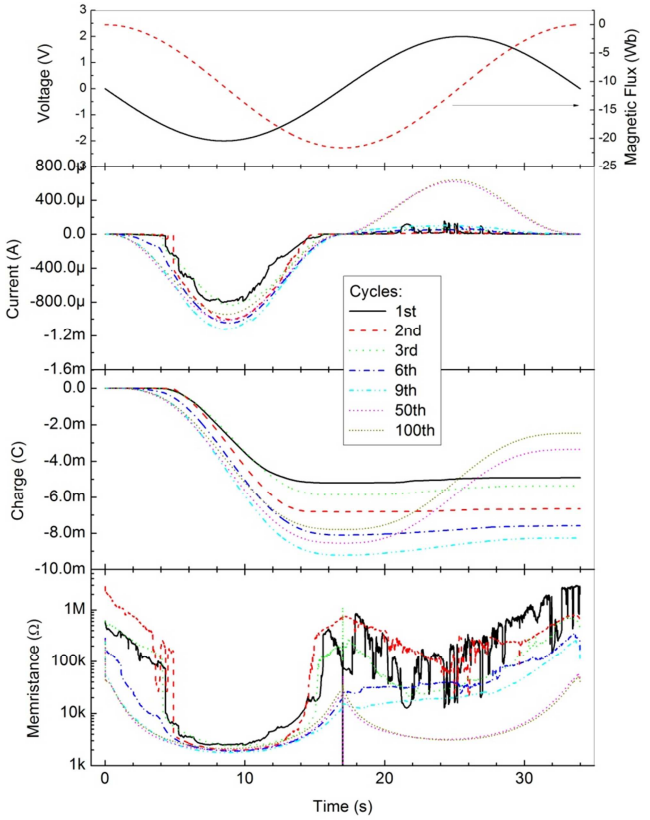

Figure 5. *The important variables plotted as functions of time during the corresponding cycles. At the top, the voltage and magnetic flux, which become the same for all the cycles described here. Next, the experimental current, the calculated charge and memristance in that order, are also plotted.*

The second graph contains the time dependence of the experimental current. The charge in the third graph was evaluated by integrating this current with respect to time for each cycle and the memristance M was obtained from the I-V data by using the memristance definition, also proposed by Chua [8]:

$$M = \frac{d\varphi}{dq} = \frac{d\varphi/dt}{dq/dt} = \frac{V(t)}{i(t)} \qquad (3)$$

The instability observed formerly in Figure 4 is also clearly seen in these plots for the current, charge and memristance. All these three variables seem to follow the driving signal more closely only in the first half of each cycle (negative part of voltage). Instead, as a result of a small current produced by the positive semi-cycle of the voltage, these variables do not behave very regularly during the first 5 cycles shown. On the other hand, during the cycles 50th and 100th, a more regular behavior is observed of all current, charge and memristance as the current tends to follow more closely the shape of the driving signal during both semi-cycles. It might be considered that some stability has been reached at the 50th cycle, since the 100th cycle is seen to follow it closely. Since the magnitude of the biasing voltage never surpassed the limiting value of 2 volts, we might say that such stability was achieved without any hard-forming process as opposite to many other memristive structures formerly reported by different authors.

Despite the above plotted time-dependences are quite illustrative regarding the evolution of the memristive structures along their electrical history, the best description of the devices is provided by using either the constitutive relationship defined as that between the charge (q) and the magnetic flux (φ) or the state map given as the relationship between charge and memristance. These relationships are depicted in Figure 6. Two branches are clearly seen in the φ vs. q plots: the first one corresponds to the negative semi-cycle of biasing where a large current is produced, related also to a large amount of charge moved along such semi-cycle; the second one reflects the small current produced by a much lower flow of charge during the positive half-cycle. It must be noticed that despite the 50th and 100th current-voltage plots look very similar, significant differences are clearly observed between the corresponding φ vs. q plots. These differences mean that the structure has not reached total stability.

The curves in the bottom figure might also be obtained by deriving those in the top in accordance with the first equality at equation (3). This relationship between both families of curves explains why in those in the bottom the instability of the first measurement cycles is clearly seen but those in the top describe such history in a much smoother way.

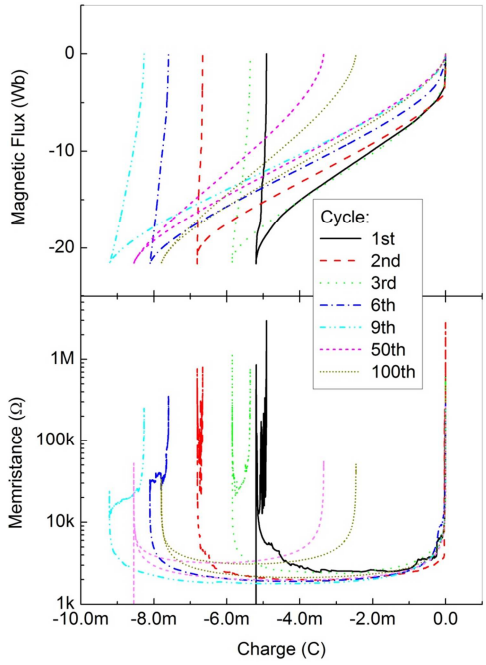

Figure 6. *Top: Plots of the so-called constitutive relationship depicting the magnetic flux dependence on the charge passing through the structure. Bottom: The state maps defined by the memristance-charge dependence, which are related to those plotted in the top.*

Again, in Figure 6 (bottom) two branches can be seen: the first one representing the change of memristance under the passage of negatively injected charge, which starts at the 0 abscissa and the other, spanning a very narrow charge range for the first cycles, corresponding to positively forced charge. During the 1st cycle, memristance changed from nearly 2 kΩ up to about 900 kΩ. Instead, according to the curves of cycles nos. 50 and 100, after the evolution of the structure, memristance can be controlled between ~ 2 kΩ and 30-50 kΩ by using both, positive and negative charge injection. Clearly, the existence of two branches in both families of curves is a consequence of the asymmetric behavior of the current-voltage plots.

4. Mathematical Fitting to the Constitutive Relationship

By applying the Levenberg-Marquardt method to the numerical data corresponding to the 100th cycle formerly presented, a double sigmoidal type equation was fitted to the Charge vs. Magnetic Flux experimental results, which becomes the inverse of the constitutive relationship. The fitting procedure used expression (4) with correlation coefficients r = 0.99997 for the negative branch and r = 0.99998 for the positive one:

$$q(\varphi) = A1 + (A2 - A1)\left[\frac{p}{1+10^{(B1-\varphi)h1}} + \frac{1-p}{1+10^{(B2-\varphi)h2}}\right] \quad (4)$$

The parameter values are given in table 1. The standard errors for all of them are quite acceptable.

Table 1. *Parameter values resulting from the mathematical fitting to the inverse function of the constitutive relationships (both branches) corresponding to the 100th cycle obtained from the experimental measurements.*

Parameter	Negative branch		Positive branch	
	Value	Standard error	Value	Standard error
A1	-0.00838	8.28115×10^{-6}	-0.00843	8.15×10^{-6}
A2	4.28672×10^{-4}	6.11566×10^{-6}	-0.00222	2.44039×10^{-6}
B1	-6.56407	0.04978	-15.29215	0.05644
B2	-15.10734	0.05142	-6.64486	0.04845
h1	0.15199	0.00131	0.12048	0.00102
h2	0.13958	0.00116	0.15892	0.00153
p	0.44745	0.00832	0.66843	0.00868

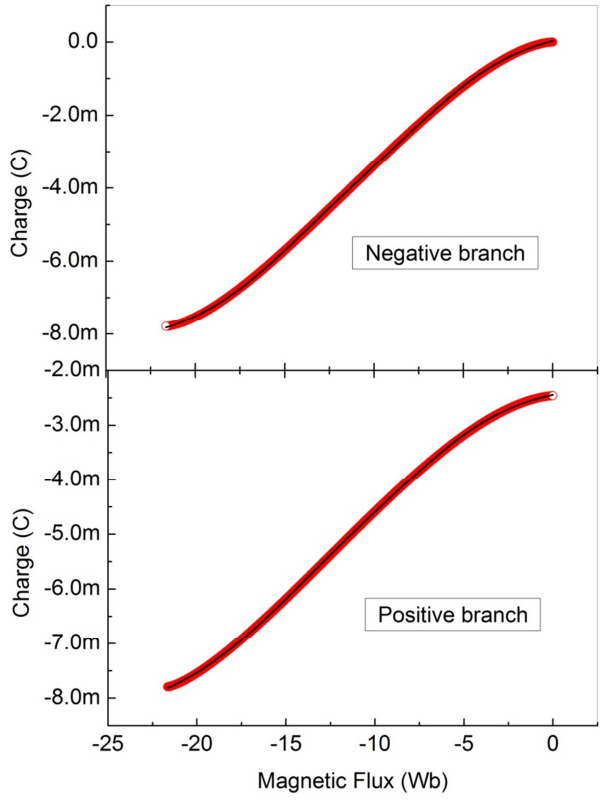

Figure 7. *Numerical fitting of a sigmoidal function to the inverse of the constitutive relationship associated to the 100th cycle of experimental data; top: negative branch; bottom: positive branch. Red symbols: experimental results; Black lines: fitted curves.*

The graphical result of the fitting procedure is seen in Figure 7 for both branches of the inverse constitutive relationship.

According to these last results, the reproducibility of the structures might be assessed according to the type of equation which best fits the q-φ data showed in Figure 7 and the values of the corresponding parameters.

5. Use of the Fitted Constitutive Relationship

As an illustration of the important information that the constitutive relationship has, we next describe the electrical behavior of the same sample under different waveforms. Namely, an appropriate simulation can be performed for any different waveform by using the above obtained q-φ relationship. As an example, the time dependences resulting from a square waveform going from -2 V up to +2 V during a similar period of 34 seconds, are presented in Figure 8.

As before, the magnetic flux can be determined directly from the voltage waveform. Then the fitted function to the constitutive relationship, equation (4) is used to find out the associated charge. By numerically deriving the charge with respect to time, the current is calculated. Finally, memristance is computed by using the current and the voltage corresponding values. It should be stressed that the memristance value can now be set up between 1.4 kΩ and 164.4 kΩ, becoming a much larger range than that under sinusoidal voltage.

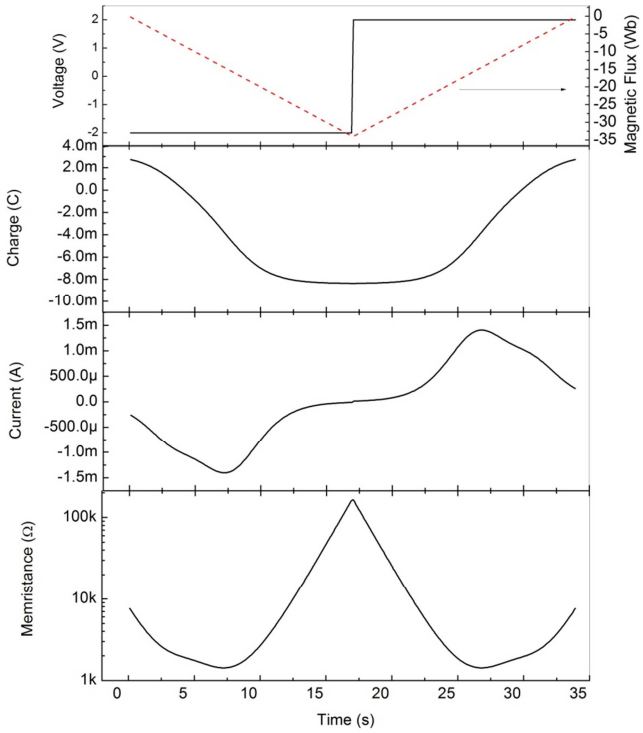

Figure 8. *Time-dependence of the variables describing the behavior of the structure, under the effect of one cycle of a 2 V square waveform.*

The whole description is completed by presenting the current-voltage plot that should be observed under this square waveform. This is shown in Figure 9 along with the results for some other cases that were also calculated for a comparison.

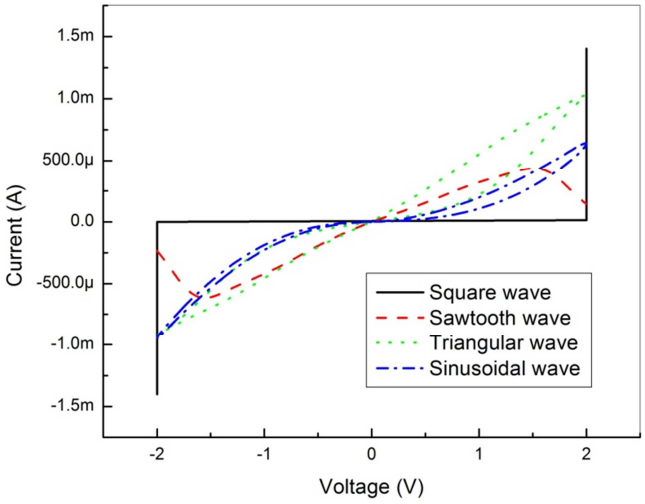

Figure 9. *Current-voltage curves for the 100th cycle that we should observe under the different 2 V amplitude waveforms.*

It can be seen from Figure 9 that the currents reached by the structure under different waveforms are in the same order, but the current-voltage curves do not coincide exactly, exhibiting each a different shape. It is then expected that also the memristance values and their time dependences differ significantly. From the corresponding calculations, the limits R_{min} and R_{max} and their ratio are shown in Table 2.

Table 2. *Memristance ranges encompassed by different waveforms having all the same amplitude (2 V) around 0 V. The sinusoidal case was determined from experimental results. The others were calculated from the first by using Chua's equations.*

Waveform	Resistance range (kΩ)	R_{max}/R_{min}
Sinusoidal	1.9 – 51.4	27.1
Square	1.4 - 164.4	117.4
Sawtooth	2.4 – 13.7	5.7
Triangular	1.8 – 16.1	8.9

Very similar R_{min} values turned out for all cases, but a significantly larger value for R_{max} in the case of the square waveform is noticeable, giving rise to a much larger memristance span as compared to other cases, corresponding to a 117.4 resistance ratio. In this sense, the most disadvantageous case corresponds to the sawtooth waveform, where only a 5.7 ratio is achieved.

We show in Figure 10 how these memristance ranges are spanned along the time during the 100st cycle.

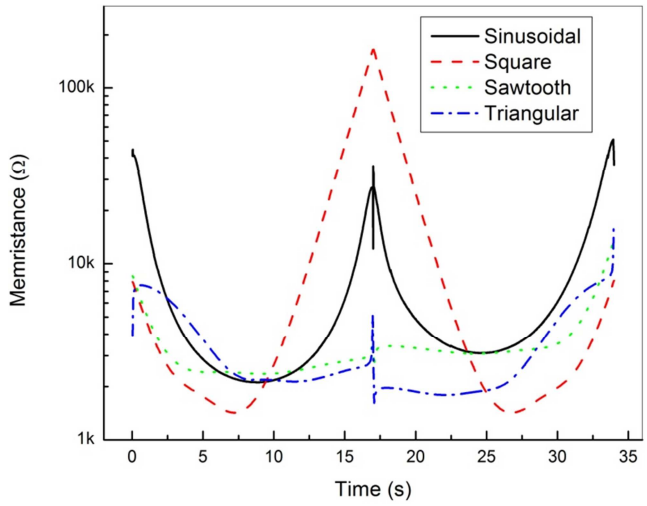

Figure 10. *A comparison of how memristance ranges are spanned by distinct waveforms having the same amplitude (2 V), during one cycle (34 s). The sinusoidal case is experimental and the others were fitted from the results of this one.*

The different resistive ranges and time-dependences resulting from distinct waveforms can be clearly seen in Figure 10. The discontinuity in the curve of the triangular case at 17 s is due to the fact that memristance is obtained from the voltage/current ratio but current in turn is the numerical derivative of charge, which is prone to a large error during calculation. Both a decreasing and increasing trends are seen for the memristance along each semi-cycle for all the waveforms shown. It is interesting to note that for the square waveform these different trends occur under constant bias: -2 V and +2 V during the first and second semi-cycles respectively. This fact suggests that different physical phenomena take place within the structure producing each trend, which will be further discussed in the second part of this work. On the other hand, exponential time dependences of the memristance are clearly seen in Figure 10, from ~5 kΩ up to R_{max} around the -2 to +2 voltage transition, close to t = 17 s. The first is an increasing trend under -2

volts and the second decreases under +2 volts. Such dependence becomes more complex between 0 and 10 s and also between 24 and 34 s. The time dependence of resistance is given as:

$$M(t) = (792.6 \pm 1.4) + (2.943 \pm 0.001) * exp\left(\frac{t}{1.55281 \pm .00006}\right) \ (10\ s \leq t < 17\ s) \quad (5)$$

Under a constant -2 V bias, but:

$$M(t) = (379 \pm 161) + (7.6 \pm 0.3) * 10^9 * exp\left(-\frac{t}{1.584 \pm 0.006}\right) \ (17\ s < t \leq 24\ s) \quad (6)$$

under a constant +2 V bias. In both expressions, the time t is given in seconds and M(t) in Ohms.

Regarding the other waveforms, such dependences are more complex.

6. Conclusion

Memristive TiOx structures based on non-uniform thermally oxidized rutile-like films could be fabricated and assessed. An oxygen-vacancy doped region of about 5 nm thickness was found in our 35 nm-thick film. The I-V characteristics were obtained under a digitized sinusoidal excitation voltage of 2 V amplitude and 29.4 mHz frequency. No hard-forming process was needed to reach stability of the structures. Achievement of stability was delayed longer under the positive voltage in the second semi-cycle. Prof. Chua's basic equations were used to obtain from this tabulated data a time-dependent description of the important variables for several measurements: charge, magnetic flux and memristance. The in-depth description of the structures is provided by the constitutive relationship: magnetic flux vs. charge and its derivative (memristance vs. charge). A double sigmoidal function reasonably fitted the inverse of the constitutive relationship. Calculations using this fitted function yielded the response to other different waveforms. In our samples, a larger memristance span was obtained from the square wavefunction as compared to those from a sawtooth, a sinusoidal and a triangular waveform. An exponential time dependence of the resistance value between 5 kΩ and 164 kΩ was determined under a ± 2 V square waveform. The functional dependence between q and φ and the values of the parameters involved can be used to assess the reproducibility of similar structures. Since only parameters depending on the experimental data are obtained, the procedure followed in this work might be used for any memristive device. Moreover, the data obtained in this way might be the base for further analysis of the structures in the light of some specific memristor model. Such analysis will be presented elsewhere.

Acknowledgements

The authors are grateful to CINVESTAV del I.P.N. for providing the resources to carry out this work.

References

[1] S. R. Ovshinsky, Reversible electrical switching phenomena in disordered structures, Phys. Rev. Lett., V. 21, No. 20, Nov. 1968, pp. 1450-1453.

[2] I. Balberg, Simple test for double injection initiation of switching, Appl. Phys. Lett., V. 16 No. 12, June 1970, pp. 491-493.

[3] W. D. Buckley and S. H. Holmberg, Electrical Characteristics and threshold switching in amorphous semiconductors, Solid-State Electronics, V. 18, 1975, pp. 127-147.

[4] H. J. Hovel, Switching and memory in ZnSe-Ge heterojunctions, Appl. Phys. Lett. V. 17, No. 4, August 1970, pp. 141-143.

[5] P. G. LeComber, A. E. Owen, W. E. Spear, J. Hajto, and W. K. Choi, Electronic switching in amorphous silicon junction devices, Semiconductors and Semimetals, Vol. 21, Part D, 1984, pp. 275-289.

[6] A. Avila G., ac measurements in non-volatile amorphous silicon memories, M.Sc. Thesis, developed at the University of Edinburgh and submitted at the University of Dundee, Scotland, Sept. 1986.

[7] D. B. Strukov, G. S. Snider, D. R. Stewart, and R. S. Williams, The missing memristor found, Nature, Vol. 453, pp. 80-83, (2008).

[8] L. O. Chua, Memristor – the missing circuit element, IEEE Trans. Circuit Theory, Vol. 18, Issue 5, pp. 507-519, (1971).

[9] S. H. Jo, K. H. Kim, W. Lu, High-density crossbar arrays based on a Si memristive system, Nano Lett. 9, 870–874 (2009).

[10] Y. Joglekar and S. Wolf, "The elusive memristor: properties of basic electrical circuits," *Eur. J. Phy.*, vol. 30, 2009, pp. 661–675.

[11] *Milka POTREBIC, Dejan TOSIC,* Application of Memristors in Microwave Passive Circuits, RADIOENGINEERING, VOL. 24, NO. 2, JUNE 2015.

[12] D. Jeong, H. Schroeder, and R. Waser, \Impedance spectroscopy of TiO_2 thin films showing resistive switching," Applied Physics Letters, vol. 89, no. 8, 2006.

[13] Reut Wizenberg, Applications of Solid-State Memristors in Tunable Filters, IEEE, 2014.

[14] B. J. Choi, D. S. Jeong, S. K. Kim, C. Rohde, S. Choi, J. H. Oh, H. J. Kim, C. S., Hwang, K. Szot, R. Waser, B. Reichenberg, and S. Tiedke, "Resistive switching mechanism of TiO_2 thin films grown by atomic-layer deposition," Journal of Applied Physics, vol. 98, no. 3, 2005.

[15] Yulia Khrapovitskaya, Natalia Maslova, Ivan Sokolov, Yulia Grishchenko, Dmitry Mamichev, and Maxim Zanaveskin, The titanium oxide memristor contact material's influence on element's cyclic stability to degradation, P hys. Status Solidi C 12, No. 1–2, 202–205 (2015) / DOI 10.1002/pssc.201400109.

[16] Y. Katsuka, S. Tanifuji and K. Yahagi, Two kinds of switching phenomena in TiO_2 thin films, Japan. J. Appl. Phys. 11 (1972) 771-772.

[17] Y.-T. Li, S.-B. Long, H.-B. Lv, Q. Liu, Q. Wang, Y. Wang, S. Zhang, W.-T. Lian, S. Liu, and M. Liu, "A low-cost memristor based on titanium oxide," 10th IEEE Int. Conf. on Solid State and Integr. Circuit Technol 2010, Nov. 2010, pp. 1148-1150.

[18] L. Ortega-Reyes, A. Ávila-García, "Thermally grown vanadium oxide films and their electrical properties", *Materials Science in Semiconductor Processing* 37 (2015) 123-128.

[19] A. Avila-Garcia, L. Ortega-Reyes, Memristive properties of thermally grown titanium and vanadium oxides, Memories of 15° Congreso Internacional de Metalurgia y Materiales, CONAMET-SAM, Concepción Chile, November 2015.

[20] J. G. Simmons, Generalized Formula for the Electric Tunnel Effect between Similar Electrodes Separated by a Thin Insulating Film, J. Appl. Phys. 34, 1793 (1963); doi: 10.1063/1.1702682.

[21] S. Kvatinsky, E. G. Friedman, A. Kolodny, and U. C. Weiser, TEAM: ThrEshold Adaptive Memristor Model, IEEE TRANSACTIONS ON CIRCUITS AND SYSTEMS—I: REGULAR PAPERS, VOL. 60, NO. 1, JANUARY 2013, pp. 211-221.

[22] M. E. FOUDA, A. G. RADWAN, ON THE FRACTIONAL-ORDER MEMRISTOR MODEL, Journal of Fractional Calculus and Applications, Vol. 4 (1) Jan. 2013, pp. 1- 7. ISSN: 2090-5858.

[23] L. Chua, Resistance switching memories are memristors, Appl. Phys. A (2011) 102: 765-783.

[24] A. Arreola-Pina, Oxido de titanio térmico para memristores, M.Sc. Thesis, CINVESTAV del I.P.N., Cd. De México, México, 2014.

[25] U. Balachandran and N. G. Eror. "Raman spectra of titanium dioxide", *J. Sol. St. Chem*. 1982: 42 276-282.

[26] M. S. Zhang, Z. Yin et al. "Raman scattering by nanophase titanium dioxide", *Ferroelectrics* 1995: 168 (1) 131-137.

[27] G. A. Tompsett, G. A. Bowmaker et al. "The Raman spectrum of brookite, TiO_2 (Pbca, Z=8)", *J. of Raman Spec*. 1995: 26 (1) 57-62.